energies

MDPI

Article

Optimal Configuration of Energy Storage Systems in High PV Penetrating Distribution Network

Jinhua Zhang [1], Liding Zhu [1,*], Shengchao Zhao [1], Jie Yan [2] and Lingling Lv [1]

[1] School of Electric Power, North China University of Water Resources and Electric Power, Zhengzhou 450045, China
[2] State Key Laboratory of New Energy Power System, School of New Energy, North China Electric Power University, Beijing 100096, China
* Correspondence: z20211050617@163.com

Abstract: In this paper, a method for rationally allocating energy storage capacity in a high-permeability distribution network is proposed. By constructing a bi-level programming model, the optimal capacity of energy storage connected to the distribution network is allocated by considering the operating cost, load fluctuation, and battery charging and discharging strategy. By constructing four scenarios with energy storage in the distribution network with a photovoltaic permeability of 29%, it was found that the bi-level decision-making model proposed in this paper saves 2346.66 yuan and 2055.05 yuan, respectively, in daily operation cost compared to the scenario without energy storage and the scenario with single-layer energy storage. After accessing IEEE-33 nodes for simulation verification, it was found that the bi-level decision-making model proposed in this paper has a good inhibition effect on voltage fluctuation and load fluctuation after energy storage configuration. In addition, this paper analyzes the energy storage that can be accessed by photovoltaic distribution networks with different permeability and finds that when photovoltaic permeability reaches 45% and corresponding energy storage is configured, the economic and energy storage benefits of the system are the best.

Keywords: high PV penetration; energy storage; optimal configuration; bi-level decision-making models

Citation: Zhang, J.; Zhu, L.; Zhao, S.; Yan, J.; Lv, L. Optimal Configuration of Energy Storage Systems in High PV Penetrating Distribution Network. *Energies* **2023**, *16*, 2168. https://doi.org/10.3390/en16052168

Academic Editors: Luis Hernández-Callejo, Jesús Armando Aguilar Jiménez and Carlos Meza Benavides

Received: 31 January 2023
Revised: 16 February 2023
Accepted: 20 February 2023
Published: 23 February 2023

1. Introduction

In recent years, with global carbon dioxide emissions hitting record highs, China has proposed a "two-carbon" target to tackle environmental problems. Promoting the development of new energy and the transformation of energy structures has become an important part of global development. Due to abundant reserves and easy access, solar energy has been developing rapidly in recent years, and its proportion in the power grid has been increasing year by year [1]. While improving energy utilization, this has brought a lot of trouble to the power distribution network. With the continuous increase in the penetration rate of photovoltaics integrated into the power distribution network, problems such as voltage collapse may occur, which has a serious impact on the safe and stable operation of the system [2].

Studies have shown that a large number of photovoltaics connected to the distribution network will also increase the number of system equipment, which will bring a burden to the system and easily generate harmonic interference. In addition, the retrograde power generated by the grid connection is prone to exceed the limit of the system node voltage, which not only reduces the power quality but also deteriorates the user experience. When high-penetration photovoltaics are connected to the grid, the uncertainty of output cannot be matched with the load of the distribution network in real-time, which will affect the power balance of the system. When the photovoltaic output fluctuates greatly due to the change in environment and climate, the stability of the system will be affected [3]. In addition, the high-penetration photovoltaic grid connection requires a large number of

power electronic equipment to join the distribution network, which leads to the existence of harmonics and affects the power quality [4], and the dispatching flexibility of the distribution network is greatly reduced, which makes it more difficult for the power system to develop a power generation plan. If such problems cannot be properly solved, it will not only seriously threaten the safe and stable operation of the system but also cause a waste of energy and limit the future development of photovoltaic power generation [5].

The authors in [6–8] analyze the influence of photovoltaic systems from the aspects of voltage fluctuation, voltage amplitude, and frequency. From the perspective of stability, Rasoul proposed a new framework to analyze the influence of different photovoltaic permeability on voltage stability [9]. During the study, Zetty found that in a high permeability renewable energy distribution network, load fluctuation is the main factor leading to the voltage fluctuation of the system, and the realization of various fluctuations in the high-light voltage permeability distribution network is important content to achieve the increase of photovoltaic permeability in the distribution network [10]. The introduction of energy storage devices improves the power quality while improving the photovoltaic stable output [11–13]. Through reasonable regulation and control of a BESS, the absorption of new energy on the power generation side can be completed, the permeability of distributed power supply on the transmission side and distribution side can be improved, and the safe, stable, and economic operation of the system can be ensured [14,15]. The authors in [16–18] studied the working principle and characteristic analysis of different types of energy storage devices and different types of BESSs and discussed the practicability of combining BESS energy storage and generation measurement. From the perspective of photovoltaic and load output prediction, Rahman and Zhao verified the feasibility of combining energy storage optimization configuration with the prediction by comparing scenarios with or without prediction [19,20]. In order to meet the photovoltaic energy storage demand in the distribution network, Wang's multiple operation scenarios of energy storage were divided into grid scenarios to obtain the demand relationship of energy storage capacity under different operating conditions and to complete the calculation of energy storage capacity [21].

Access to energy storage equipment requires considerable capital investment in actual project construction and operation and maintenance. Therefore, the demand response for energy storage capacity is important content in optimizing energy storage configuration. In [22], Balouch proposed an optimization goal of matching demand and supply. Based on the analysis of line planning, low-cost scheduling, and demand response, the energy utilization efficiency and comprehensive operating cost of a smart grid were optimized. The authors in [23,24] introduced the improved optimization algorithm to improve the optimization ability so as to determine the optimal scheme of energy storage optimization configuration and realize a higher degree of response between demand and supply by analyzing various indicators of access to the power grid. In [23], Balouch optimized a response scheduling scheme by introducing the GWCSO algorithm. Higher robustness and computational efficiency of the algorithm make the optimization results more advantageous in power cost and peaking ratio. In [24], Mostafa improves the PSO algorithm, improves the accuracy and effectiveness of the algorithm, and optimizes the location and capacity allocation of energy storage in distributed networks. While the optimization objects are complex and diverse when connecting to the power system, the choice and update of the Pareto optimal solution will determine the quality of the final optimization result [25].

In the existing studies, it seems obvious for everyone to apply energy storage in high-permeability photovoltaic distribution networks [26–32]. In the case of low photovoltaic permeability, access to energy storage can indeed improve photovoltaic output and power quality. However, few researchers have analyzed whether energy storage can still meet expectations in the scenario of high photovoltaic permeability, and how to rationally allocate energy storage in a distribution network with high photovoltaic permeability. In this paper, the application of energy storage in a high permeability photovoltaic scenario is analyzed, and the energy storage in a high-light volt distribution network is configured by

establishing a two-layer planning model of the distribution network. The optimal size of energy storage was configured considering the fluctuation of power grid voltage and load, economic benefits and energy storage benefits, and the working condition of energy storage in the scenario of high-light voltage permeability, and the improvement of benefits in all aspects of the distribution network were studied. Finally, the feasibility of the proposed method was verified in the IEEE-33 node system.

The main contributions of this study are summarized below:

- Proposed a method for optimal allocation of energy storage capacity of a distribution network based on a two-layer programming model and verified its feasibility.
- Used the K-means method to complete an analysis of the uncertain photovoltaic output into the deterministic scenario.
- The multi-objective particle swarm optimization algorithm was improved to solve the optimal configuration, and the advantages of the improved algorithm were compared.
- By constructing different scenarios, it was verified that energy storage can still improve the power quality in the distribution network with high-light voltage and permeability.
- Through analysis of the optimal configuration of energy storage in the distribution network with different photovoltaic permeabilities, the optimal economic photovoltaic permeability was concluded.

The rest of this paper is organized as follows: The treatment method for the PV uncertainty and the selection of the PV working curve is introduced in Section 2. In Sections 3 and 4, the bi-level decision-making programming model is constructed and solved to realize the addressing and capacity selection of the energy storage device. At the same time, in the fourth section, the specific content of particle swarm optimization is described. In Section 5, four scenarios are constructed to discuss the benefits generated by energy storage configuration and optimization benefits brought by algorithm improvement. Finally, in Section 6, we summarize the content of the thesis.

2. Analysis of Photovoltaic Output Characteristic

Due to the great influence of light and the environment, photovoltaic power generation is full of uncertainties. For further analysis, we collected the annual daily output data of photovoltaic power stations (annual output of an operational photovoltaic power station in Henan Province from June 2019 to July 2020), as shown in Figure 1. When considering energy storage benefits, excessive uncertainty in output will lead to uncertainty in energy storage benefits. In order to avoid this influence, this paper will process various output curves by clustering the division method, summarizing the photovoltaic output with high uncertainty into six typical output scenarios and analyzing them, and transforming the uncertainty into a deterministic analysis.

2.1. K-Means Cluster Analysis Method

The K-means clustering method is a classical clustering analysis method based on the iterative method which has the advantages of high efficiency and convenience in processing large-scale uncertain data [33]. Through the K-means clustering method, a large number of output data can be refined and extracted, and fewer typical output scenarios can be obtained that can represent the output of photovoltaic power stations.

The K-means algorithm sets an initial cluster center in all scenes and iterates clustering for a large number of scenes based on the optimal distance. The iteration is not finished until the clustering presents a steady-state equilibrium. The iteration results are shown in Figure 2. After the whole process is complete, the center of each cluster scene is set as the partition scene, and the probability of each cluster scene is set as the required partition probability $P_r(s)$.

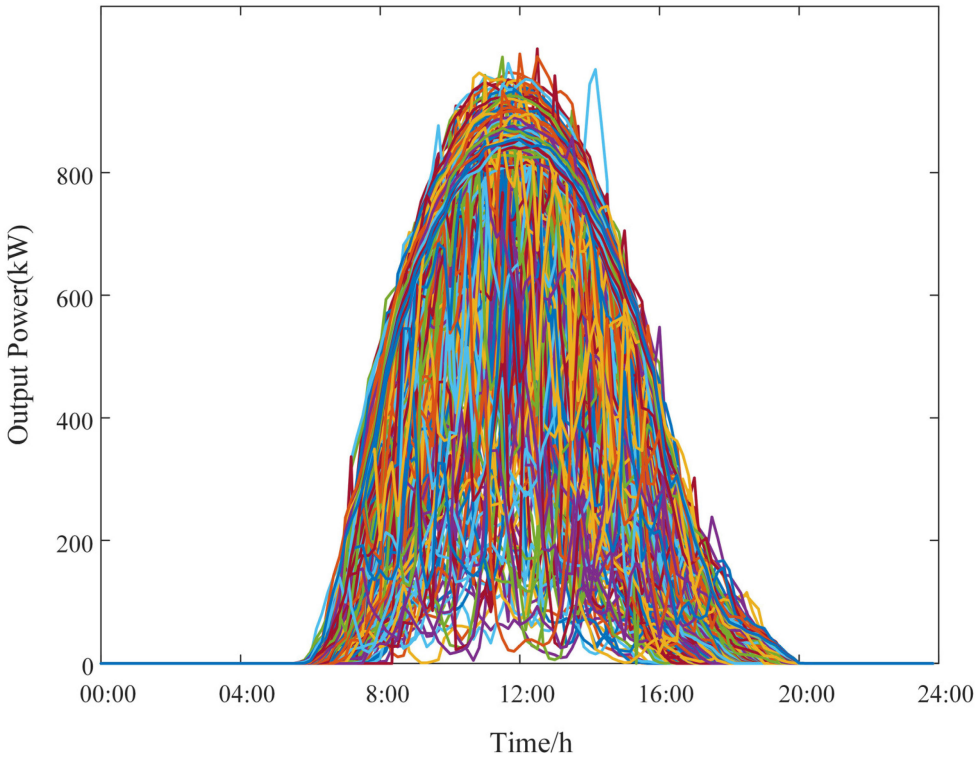

Figure 1. Annual daily output curve of photovoltaic power plants.

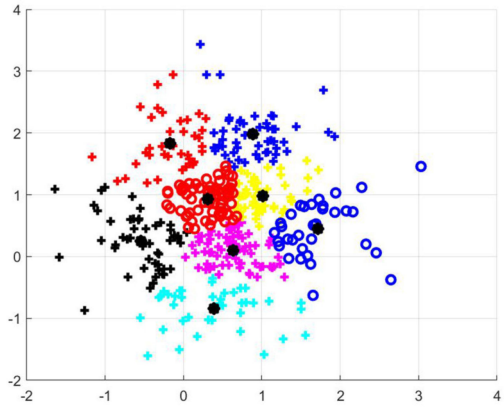

Figure 2. K-means clustering method results.

Set the number of initial scenarios $\xi_s (s = 1, 2 \ldots N)$ to N_s. The number of target scenarios is M_s, and the entire calculation procedure is as follows:

① M_s target scenes with random data are set as the cluster center, and the set of these scenes is $Center = \left\{\xi_s^{Center}\right\}$ $(s = 1, 2 \ldots M_s)$.

② Excluding the cluster center set, the other scene set is set as $Member = \{\xi_s^{Center}\}$ $(s = 1, 2 \ldots M_s)$, and the distance from the other scene set to the cluster center scene set is calculated: $\begin{cases} DT_{s,s'} = DT\left(\xi_s^{Center}, \xi_s^{Member}\right) = ||\xi_s^{Center} - \xi_s^{Member}||_2 \\ s = 1, 2 \ldots M_s \, , s' = 1, 2 \ldots N_s - M_s \end{cases}$

③ The other scene sets excluding the cluster center set are divided into the nearest cluster center according to the distance calculated in ②. We obtain the cluster set $Cluster = \{C_i\}, i = 1, 2 \ldots M_s$, where C_i is a set of similar scenarios.

④ Set the same cluster C_i including L_s scenarios. Add the distances from each scenarios to the others: $CT_s = \sum_{\substack{s'=1 \\ s' \neq s}}^{L_s} ||\xi_s - \xi_{s'}||_2$, and scene ξ_k in $CT_s = Min(CT_s)$ is selected as

the clustering center of the next iteration. This is used to calculate the next iteration cluster center set.

⑤ At this point, stable cluster centers and clustering results can be obtained by repeating steps ②–④. The probability number of each type of scenario is the probability number of a single scenario in that type of scenario.

The process of the clustering algorithm to reduce the scene is shown in Figure 3.

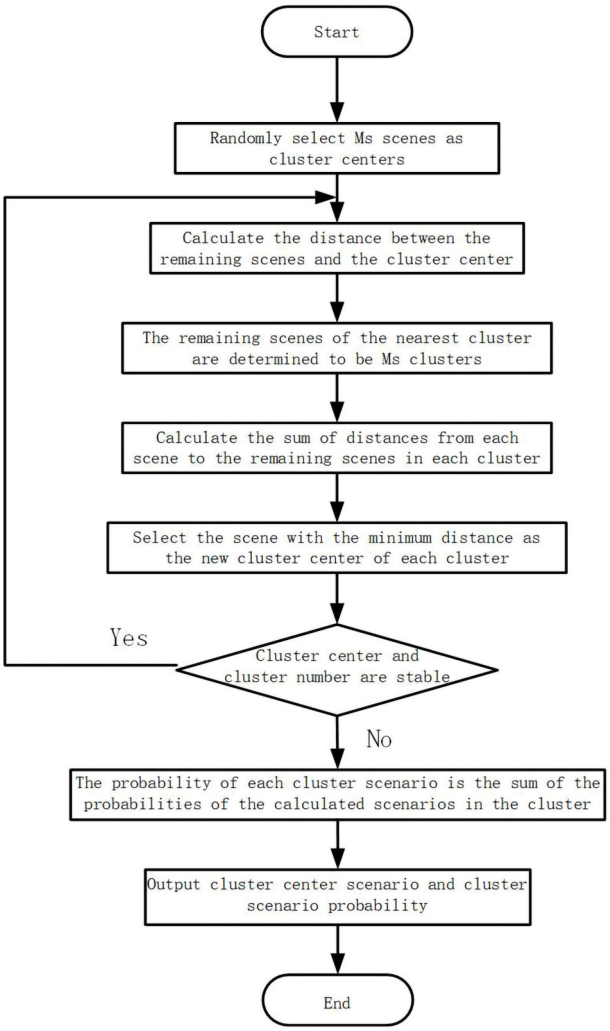

Figure 3. Cluster reduction flowchart.

2.2. Selection of Typical Output Scenarios

After data processing and division by the K-means clustering method, six output scenarios as shown in Figure 4 can be obtained. The occurrence probability and the number of curves of each output scenario are shown in Table 1.

Table 1. Typical scenario probability.

Scenario	Number of Curves	Probability	Scenario	Number of Curves	Probability
1	35	0.0959	4	24	0.0658
2	7	0.0192	5	127	0.3479
3	75	0.2055	6	97	0.2658

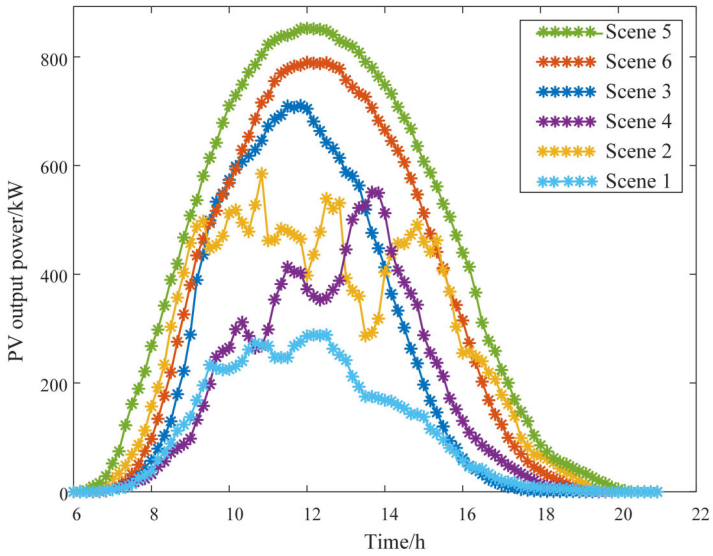

Figure 4. Clustering of typical scenarios.

As can be seen from Figure 4 and Table 1, the photovoltaic output power in Scenario 1 is low, while the output in Scenario 2 has great fluctuation and uncertainty. The intermediate level of output in Scenarios 3 and 4 cannot represent photovoltaic output, and Scenarios 5 and 6 have a high probability and good output curve. In contrast, Scenario 5 with the maximum annual output is selected as the typical photovoltaic output curve, which can better reflect the output characteristics of photovoltaic power generation. In order to facilitate the analysis of the combined effect of photovoltaic and energy storage under different permeability, in this paper, we will only select Scenario 5, which is the most representative and has the highest probability of occurrence at the same time, as the analysis object to study the influence of energy storage access to the power grid during daily operation on voltage fluctuation, operation cost, and other benefits of the distribution network.

3. BESS Bi-Level Decision-Making Model Configuration

Due to the mutual influence between the optimal configuration of the energy storage system and the stable operation of the distribution network, this will bring difficulties to the dispatching of the energy storage devices and will cause the operation stability of the distribution network to decline. Therefore, it is necessary to consider a reasonable location and capacity while taking into account the operation economy of the distribution network. The bi-level decision-making model relies on its own two-level hierarchical structure to optimize the system objectives hierarchically. The upper and lower levels influence each other and seek the overall optimal solution according to the independent objective function and the corresponding constraints [34,35].

3.1. Upper-Level Model Objective Function

In the upper-level optimization, energy storage configuration location, rated power, and installed capacity are considered to reduce the total cost of the energy storage system and distribution network investment and maintenance. The installation location and capacity of the BESS are optimized. After the optimal configuration of energy storage is obtained, the information is transmitted to the lower level to adjust the charge and discharge power of energy storage.

$$\begin{cases} F_{min} = f_{sto} + f_{ope} \\ s.t. g(X) \leq 0 \end{cases} \quad (1)$$

where F_{min} is the minimum daily total cost after the energy storage is connected; f_{ope} is the total cost of distribution network operation investment. f_{sto} is the input costs for energy storage construction. $X = [x_1, x_2, x_3]$, and x_1, x_2, x_3, respectively, represent the BESS input node, power, and capacity.

3.2. Lower Objective Function

In the lower-level optimization, due to the influence of the energy storage installation location and capacity selection on the energy storage life, the lower-level decision-making model fully considers the change of the energy storage charging and discharging power to realize the economical operation mode of the distribution network and achieve the smallest fluctuation range of node voltage and load. The lower optimization objective function is as follows:

$$\begin{cases} min(f_{ope}, f_2, f_3) \\ s.t.h(y) \leq 0 \end{cases} \tag{2}$$

where f_2 is the amplitude of the voltage fluctuation of the distribution network node caused by the access to energy storage, f_3 is the amplitude of the load fluctuation of the distribution network, and $y = [y_1, y_1, y_2 \ldots y_{24}]$ is the average hourly charging and discharging power of the energy storage system throughout the day.

(1) The voltage fluctuation of distribution network nodes caused by energy storage access can be expressed as:

$$min\ f_2 = \sum_{t=1}^{24} \sum_{k=1}^{N} \left[\frac{u_k(t) - u_{kn}}{\Delta u_{kmax}} \right]^2 \tag{3}$$

where N indicates the number of system nodes, and $u_k(t)$ indicates the voltage value of node k at time t.

(2) The load fluctuation of the distribution network caused by access to energy storage can be expressed as:

$$min\ f_3 = \frac{1}{T} \sum_{t=1}^{T} \left[P'_{load}(t) - P'_{ave} \right]^2 \tag{4}$$

where P'_{ave} represents the average load in a period of time when energy storage is connected.

3.3. Constraints

(1) Constraints at the BESS access node

$$1 \leq x_1 \leq N_{max} \tag{5}$$

where x_1 are nodes invested in energy storage, and N_{max} is the maximum number of nodes expressed as energy storage input.

(2) The constraints of power rating and capacity energy storage devices can be expressed as

$$\begin{cases} P_{ess}^{min} \leq P_{essn} \leq P_{ess}^{max} \\ E_{ess}^{min} \leq E_{essn} \leq E_{ess}^{max} \end{cases} \tag{6}$$

where P_{ess}^{max} and P_{ess}^{min} is the maximum and minimum value of the rated output of the energy storage, and E_{ess}^{max} and E_{ess}^{min} are the maximum and minimum values of the energy storage input capacity.

(3) Power balance constraints

$$P_{grid} + P_{gv} = P_{load} + P_{loss} + P_{ess} \tag{7}$$

where P_{grid} is the power value received by the grid, P_{gv} is the PV output power, P_{load} is the output power, P_{loss} is the network loss, and P_{ess} is the BESS input power.

(5) BESS charge and discharge power constraints

$$\begin{cases} 0 \le P_{ess}^{cha}(t) \le P_{essn} \\ -P_{essn} \le P_{ess}^{cha}(t) \le 0 \end{cases} \tag{8}$$

(6) Voltage constraints in distribution network nodes

$$u_k^{min} \le u_k(t) \le u_k^{max} \tag{9}$$

where u_k^{min} and u_k^{max} are the minimum and maximum voltages of node k at time t. Energy storage system SOC constraints

$$SOC(t) = \frac{E(t)}{E_{sn}} = SOC_0 + \frac{\sum_{k=1}^{t}\left\{d_1(t)P_{ess}^{cha}(t)n_c\right\}\Delta t + \sum_{k=1}^{t}\left\{d_2(t)P_{ess}^{cha}(t)/n_d\right\}\Delta t}{E_{ssn}} \tag{10}$$

where SOC_0 is the initial state of the energy storage system, including power and capacity. E_{ssn} is the rated capacity of the energy storage battery.

(7) Supplementary constraints

① Due to the limitation of the SOC range of the BESS, there will be a large number of infeasible solutions during the recovery of its all-day charging and discharging power. If its charge and discharge power is processed, this will greatly improve the convergence rate in the solution process and reduce the amount of calculation.

$$P'_{ess} = \begin{cases} P_{ess}(t)\ SOC_{min} \le SOC(t) \le SOC_{max} \\ 0\ otherwise \end{cases} \tag{11}$$

where $P'_{ess}(t)$ is the energy storage charge and discharge power value that has been processed at time t. In this way, the infeasible solution is transformed into an effective feasible solution, and the charging and discharging power that is not within the SOC range of the energy storage is changed to 0.

② Using the penalty function method to deal with the constraints that are not within the valid range:

$$F(x, M) = f(x) + M\sum_{i=1}^{r} max(g_i(x), 0) - M\sum_{i=1}^{s} min(h_i(x), 0) + M\sum_{i=1}^{t}|k_i(x)| \tag{12}$$

where M is the penalty coefficient. $g_i(x)$ indicates the negative inequality constraint. $h_i(x)$ indicates the positive inequality constraints. $k_i(x)$ indicates the equality constraint at zero. r, s, t are the number of constraints.

4. Solution of Model

For the bi-level programming model, this paper selects the genetic algorithm (GA) for the optimization of the upper layer and improved multi-objective particle swarm optimization (IMOPSO) for the optimization of the lower level. The calculation process is as follows:

① Input the demand parameters of the distribution network into the system.

② Initialize the decision variables for the upper level (including BESS installation location, power rating, and capacity). Under the constraint, the population and other parameters of the GA algorithm are initialized.

③ Initialize the decision variables of the lower level, including the BESS charge–discharge method. Under its constraints, the IMOPSO algorithm population and other related parameters are initialized to solve the initial fitness of each optimization objective.

④ After the optimization of the lower layer is completed, the TOPSIS multi-attribute decision-making method is used to select the upper Pareto solution set obtained, and

the best scheme is selected and fed back to the upper layer to solve the fitness of the upper layer target.

⑤ The upper-level GA algorithm population is updated, and the third and fourth steps are continuously executed until the upper-level optimization is completed.

⑥ The optimal BESS configuration scheme of the upper layer, the corresponding optimal charge-discharge method of the lower layer, and the optimal Pareto solution set are obtained.

The calculation process is shown in Figure 5. In the following sections, we will give a specific description of the improvement content of the multi-objective particle swarm optimization.

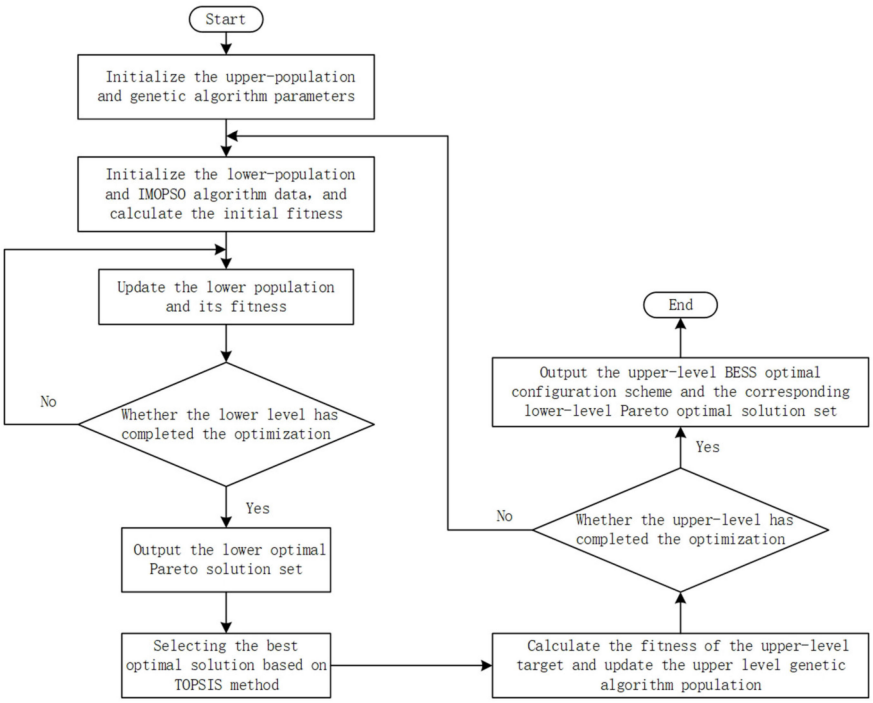

Figure 5. Calculation process.

4.1. Improved PSO Algorithm

The particle swarm optimization (PSO) algorithm is an iterative optimization algorithm. By converting the target into a certain number of particles, the position is updated in each iteration, and the optimal solution is searched through continuous iteration. The updating method is as follows:

$$v_{id}^{k+1} = wv_{id}^{k} + c_1 r_1 \left(p_{id}^{(k)} - x_{id}^{(k)} \right) + c_2 r_2 \left(g_d^{(k)} - x_{id}^{(k)} \right) \tag{13}$$

$$x_{id}^{(k+1)} = x_{id}^{(k)} + v_{id}^{(k+1)} \tag{14}$$

where w represents inertia weight; c_1, c_2 are acceleration coefficients of particle motion respectively. r_1, r_2 are randomly selected in the range of 0 to 1; $P_{id}^{(k)}$ represents the d-dimensional component of the particle numbered i in the optimal position vector at time k; and $g_d^{(k)}$ represents the d-dimensional component of the optimal position of all particles at time k.

In the process of iterative optimization, the traditional muti-objective particle swarm optimization algorithm is prone to fall into local optimal and appear 'Premature conver-

gence'. Therefore, this paper cross-mutates the prescribed bit vectors of particles to prevent them from falling into the local optimum.

$$X_{i,d} = X_{min} + (X_{max} - X_{min})r \tag{15}$$

where X_{min} represents the minimum position variable of the particle; r represents any value between 0 and 1.

Random cross variation is carried out when the probability distribution $P < P_m$ is satisfied. When the fitness of particles tends to be the same or locally optimal, the w will increase. Otherwise, the w will decrease as the particles tend to disperse [36].

$$w = \begin{cases} w_{max} - \frac{(w_{max} - w_{min})(f_i - f_{avg})}{f_{max} - f_{avg}} & f_i \geq f_{avg} \\ w_{max} & f_i \leq f_{avg} \end{cases} \tag{16}$$

where f_i is the fitness value of the particle i, w_{max},w_{min} are the maximum and minimum of w, and f_{max},f_{min},f_{avg} are the average and maximum, minimum, and average fitness of all particles at present, respectively.

In order to make the optimal solution distributed evenly in a certain range, the Pareto solution set should be optimized step by step. In this paper, a dynamic image Pareto solution set updating method is adopted, as is shown in Figure 6. In the initial distribution stage of particles, referring to all particles of the original comparison rule, an image V_{iD} is established with the optimal particle as an optimal Pareto solution set. With the progress of iteration, the average value of particles is obtained between every two images, and the optimal solution is used to make the speed and position of particles updated at this time so that the particle population moves towards the target direction. In the whole process, new particles constantly exchange information with image particles and update data in image particles continuously until the end of iteration:

$$V_{iD}^{t+1} = wv_{iD}^{t+1} + c_1 rand_1\left(p_{iD} - X_{iD}^{t+1}\right) + c_2 rand_2\left(Average\left(pbest_p\right) - x_{iD}^{t}\right) \tag{17}$$

$$x_{iD}^{k+1} = x_{iD}^{k} + v_{iD}^{k+1} \tag{18}$$

where t is the number of iterations; D is the dimension of the decision variable; p_{iD} is the best historical value of single particle i; and $pbest_p$ is the optimal particle of the current Pareto solution set in the image. $Average\left(pbest_p\right)$ is the superior particle of the optimal Pareto solution set in the two images.

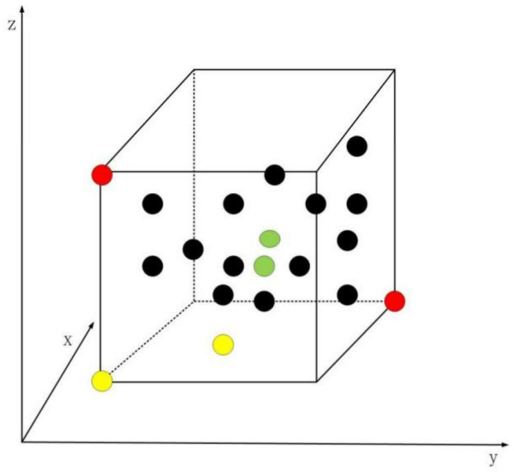

Figure 6. Dynamic image Pareto solution updates schematic.

There are differences in the selection of the optimal solutions between the multi-objective particle swarm optimization and single-objective particle swarm optimization, and the results obtained are complementary dominated Pareto solutions, which cannot be obtained by direct comparison of the particle fitness function. Therefore, in this section, the first 20% Pareto solutions with lower crowding distances and higher priority orders are randomly selected to guide the iterative updating of the particle population.

4.2. Multi-Attribute Decision-Making Based on TOPSIS Method

After solving the lower multi-objective optimization problem, the optimal solution obtained by the IMOPSO algorithm is a set of Pareto solutions, and the selection of the optimal solution is essentially a multi-attribute decision problem. TOPSIS is a method for ordering by similarity to an ideal solution, it selects the optimal solution set and the worst solution set through the established initial decision matrix, then compares the distance between the two solution sets and the evaluation index with the optimal solution set and finally sorts them to evaluate the pros and cons of the scheme. The TOPSIS method has high strict requirements in selecting weights. In this paper, the information entropy method is used to determine the weight of each target value. The information entropy method determines w by the difference of the target value in the Pareto solution, improves the accuracy of the final decision, reduces the difference, and ensures the objectivity of the decision. By using the TOPSIS method, we can determine a set of optimal Pareto solutions to guide us to choose an energy storage configuration scheme.

The optimal solution of the Pareto solution set obtained is selected from $X_1 \sim X_N$ and combined into N alternative schemes. The scheme X_i is selected from N records. It is the composition of some optimal solutions in the Pareto solution set. $g_m(X_i)$ represents the value of the mth attribute of the scheme X_i. Since each attribute is different, it should be unified and changed into the same type. The new attribute value is $G_m(X_i)$, which can be expressed as:

$$G_m(X_i) = \frac{g_m(X_i)}{\sqrt{\frac{1}{N}\sum_{i=1}^{N} g_m^2(X_i)}} \tag{19}$$

$$d(x_i) = \frac{d_+(x_i)}{d_+(x_i) + d_-(x_i)} \tag{20}$$

$$d_+(x_i) = \sqrt{\sum_{m=1}^{n} \left[\lambda_m g'_m(x_i) - \lambda_m g'_{m+}\right]^2} \tag{21}$$

$$d_-(x_i) = \sqrt{\sum_{m=1}^{n} \left[\lambda_m g'_m(x_i) - \lambda_m g'_{m-}\right]^2} \tag{22}$$

where $d(x_i)$ is the relative distance of scheme x_i; $d_+(x_i)$ represents the distance between scheme x_i and the optimal solution. $d_-(x_i)$ represents the distance from solution x_i, the negative worst solution. λ_m indicates the weight value of $g_m(X_i)$, which is randomly set between 0 and 1. g'_{m+} and g'_{m-} indicate the optimal and worst values of all schemes g_m.

5. Analysis and Discussion

5.1. Case Description

In this paper, the proposed scheme is tested on the IEEE-33 node distribution network [37]. In addition, the structure of the system is shown in Figure 7.

In this paper, the rated voltage of the selected distribution network is 12.66 kV, and the total load is 3715 kW + j2300 kvar. The upper and lower limits of the node voltage are specified as not exceeding ±5% of the rated voltage. Node 1 is a balance node, which is connected to the upper-level distribution network for power transmission. Taking into account the actual work and construction of photovoltaic power generation connected to the distribution network, photovoltaic power generation is connected to Node 9, and its installed power generation capacity is 1.077 MW (29% penetration rate).

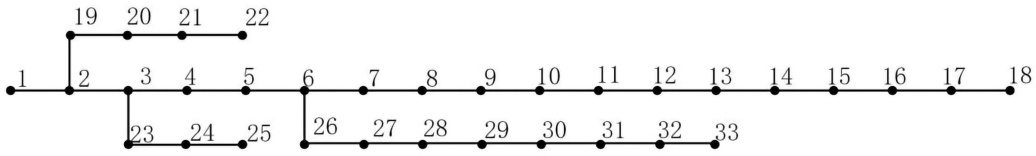

Figure 7. The topology diagram of IEEE-33 bus system.

The typical PV output curve selected by the method in Section 2 is shown in Figure 8. The typical daily load curve in this area is shown in Figure 9.

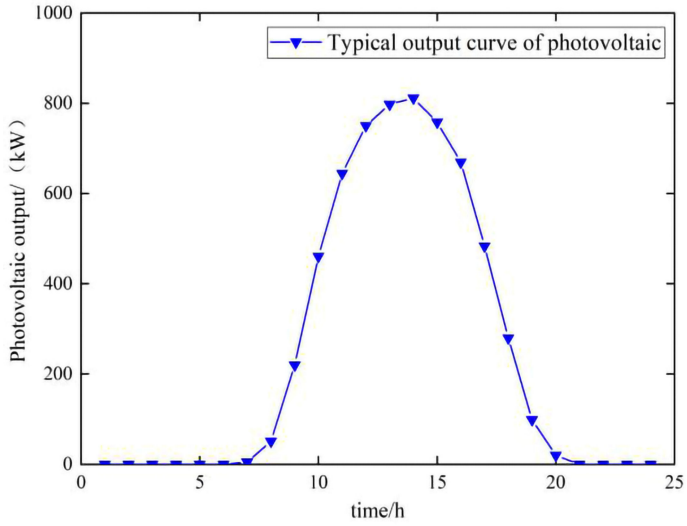

Figure 8. Photovoltaic typical sunrise force curve.

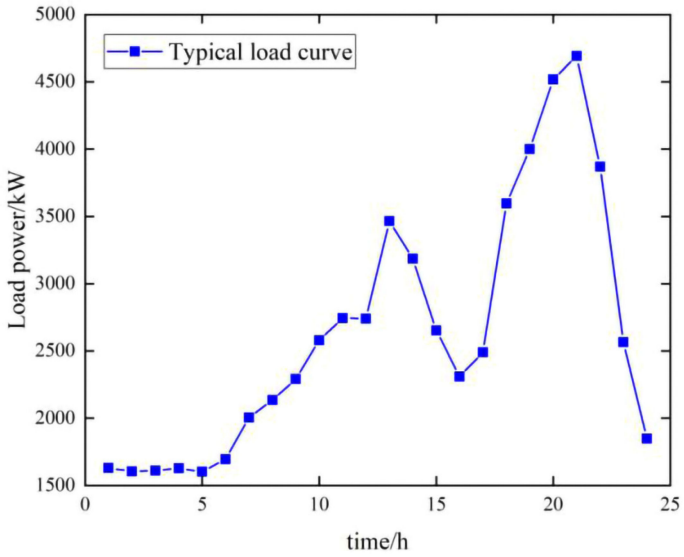

Figure 9. Typical daily characteristic curve of load.

In this paper, the battery is used as the energy storage system for research and introduces the time-of-use pricing strategy proposed in [38]. The specific time-of-use price is shown in Table 2. The energy storage control parameters are shown in Table 3. The specific setting parameters of the energy storage configuration optimization simulation are shown in Table 4.

Table 2. Time-of-use electricity price table.

Type	Period	Electricity Price (yuan/kWh)
Peak time	17:00–22:00	0.9796
Normal time	8:00–17:00 22:00–00:00	0.6570
Trough time	00:00–8:00	0.35

Table 3. Energy storage control parameter table.

Energy Storage Control Parameters	Data
Service life (year)	11
Discount Rate	0.02
Rated power cost (yuan/kW)	1000
Installation cost (yuan/kW)	2500
Operation and maintenance cost (yuan/kW)	0.05
State of charge SOC range	20–90%
Rated power upper limit (MW)	1
Maximum installed capacity (MWh)	5

Table 4. Simulation parameter settings.

Parameter	Data
Power purchase cost of grid	0.35
Expansion cost	1000
Expansion annual profit margin	8%
Load annual growth rate	1.5%
Genetic algorithm population size/number of iterations	60/200
IMOPSO algorithm population size/number of iterations	100/200
Crossover/variation rate	0.1/0.05
Inertia weight range	0.4–0.9
Threshold for difference X	0.1
The size of the Pareto solution set	100

In order to study the actual effect of energy storage configuration, we first analyzed the specific benefits of a photovoltaic distribution network connecting to energy storage configuration and demonstrated that energy storage still has good benefits in the high-light volt distribution network. Then, we compared the photovoltaic distribution network scenarios under different permeability and analyzed and compared the change of photovoltaic permeability with the corresponding change of optimal energy storage configuration scheme. The specific analysis content is introduced in the following section.

5.2. Energy Storage Optimization Scenario Division

Analyze the effectiveness of the method proposed in this paper, set different conditions, divide it into four scenarios, and compare them one by one to verify the feasibility of the method:

Scenario 1: No energy storage.

Scenario 2: With access to energy storage, use the IMOPSO algorithm in this paper to solve the optimization objective of lower-level model in the bi-level decision-making model; introduce the charging and discharging strategy of the energy storage system to simulate and analyze it.

Scenario 3: When solving its single-level model, ignore the charging and discharging management strategy of energy storage in the lower model, and only the energy storage system and distribution network are considered to have the lowest total cost. At the same time, in the time-of-use electricity price model, the energy

storage system is charged and discharged at a constant power regardless of the high or low electricity price.

Scenario 4: The optimal configuration result of energy storage in Scenario 2 is used as the constraint condition of this scenario, and the traditional multi-objective PSO algorithm is used to simulate and analyze the lower model in the optimal configuration model of the energy storage double-level. Node voltage curves and load curves in different scenarios are shown in Figures 10 and 11 below, and Table 5 shows the optimization results of different scenarios.

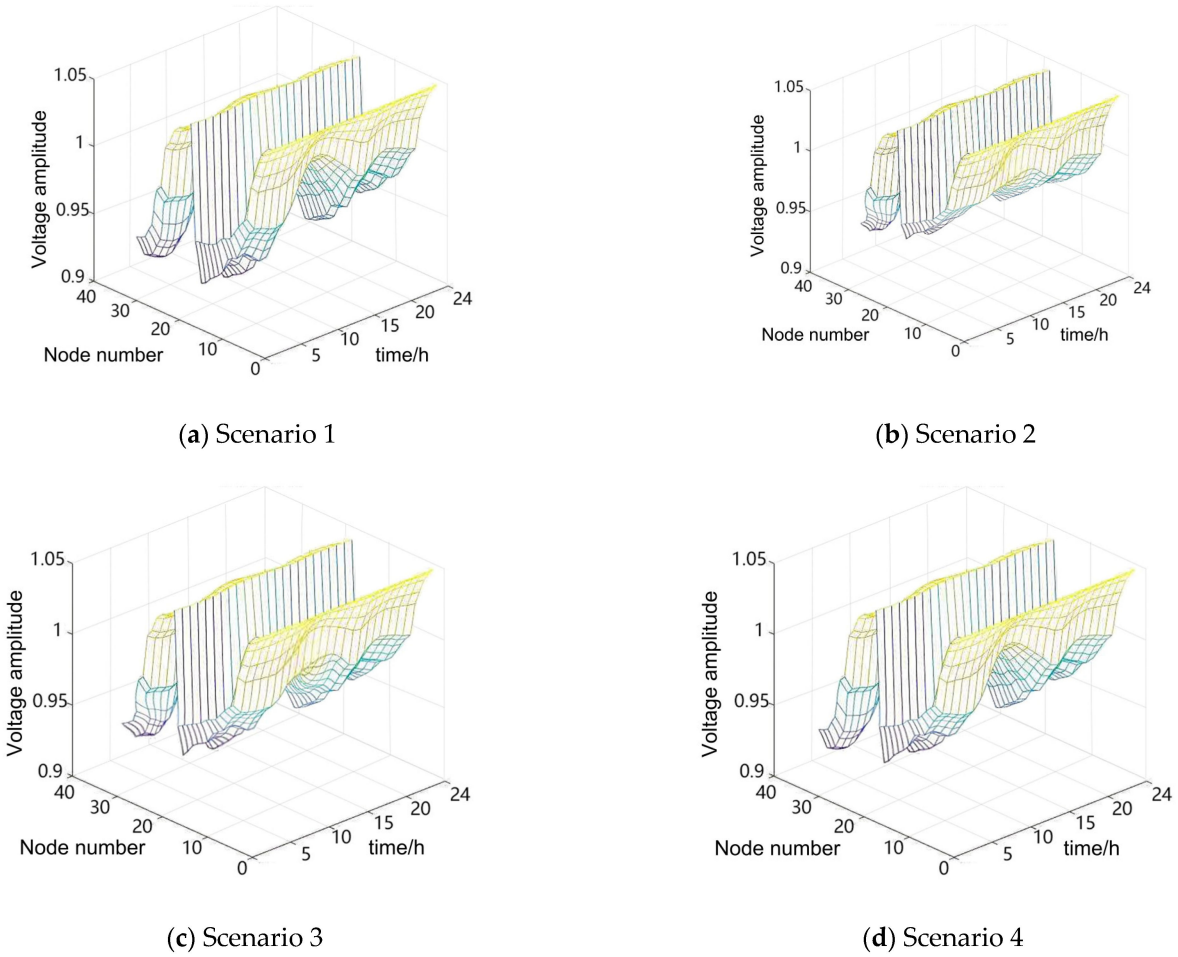

(**a**) Scenario 1 (**b**) Scenario 2

(**c**) Scenario 3 (**d**) Scenario 4

Figure 10. System node voltage curve in different scenarios.

Table 5. Optimization results in different scenarios.

Scenario	Node/Power (kw)/Capacity (kwh)	Cost of Investment	Distribution Network Operating Costs (Yuan)	Voltage Fluctuation Value	Load Variance	Total Cost (Yuan)	Degrees of Savings
1	-	0	16,703.6	70.21	36,5721.76	16,703.6	1.77%
2	14,650,3392	1879.32	14,532.67	63.52	15,3971.12	16,411.99	0%
3	20,273,2733	1497.62	15,717.64	64.98	24,9754.21	17,215.26	4.89%
4	14,650,3392	1879.32	14,767.71	64.85	15,9894.09	16,647.03	1.43%

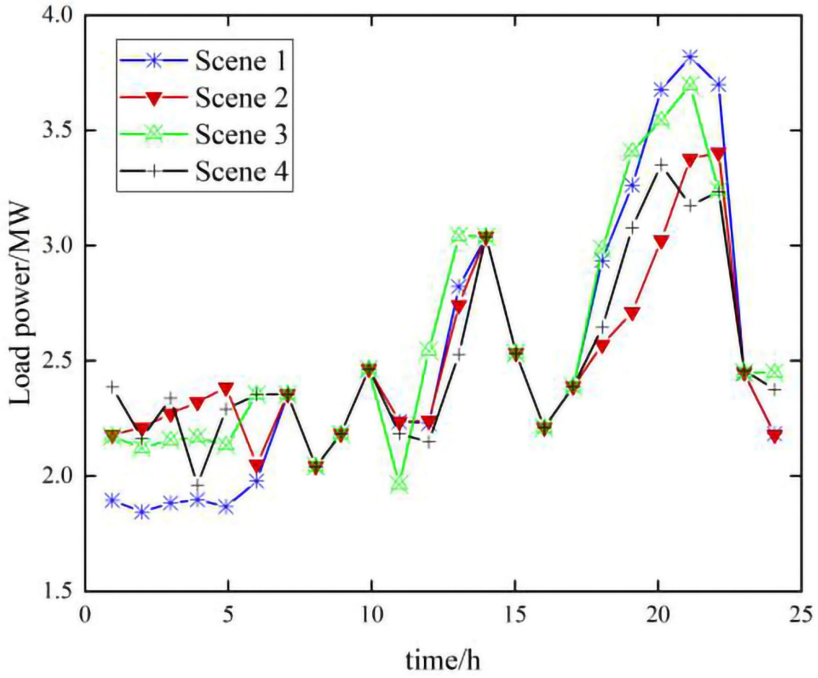

Figure 11. Load curve in different scenarios.

By comparing Scenario 1 and Scenario 2, it can be found that the voltage amplitude curve of the photovoltaic distribution network is smoother after the energy storage is connected, and the voltage fluctuation and load fluctuation are reduced to a large extent, which indicates that the BESS plays a good role in suppressing the node voltage fluctuation and load fluctuation when it is connected to the distribution network. Compared with Scenario 3, the load fluctuation range of Scenario 2 is smaller, and the load smoothing capacity is better. At the same time, the total cost of Scenario 2 is 803.27 yuan lower than that of Scenario 3 economically, which verifies the good characteristics of the model proposed in this paper.

The optimal Pareto solution set distribution of Scenario 2 and Scenario 4 is shown in Figure 12. Scenario 2 adopts the improved IMOPSO algorithm in this paper to solve the inner model, and Scenario 4 adopts the unimproved MOPSO algorithm to solve it. The Pareto solution set in Scene 2 is more evenly distributed than that in Scene 4 due to the introduction of particle cross mutation, adaptive inertia weight, and the Pareto solution set update method of the dynamic image. Moreover, Scene 2 adopts multi-attribute decisions based on the TOPSIS method, resulting in a more diverse solution set.

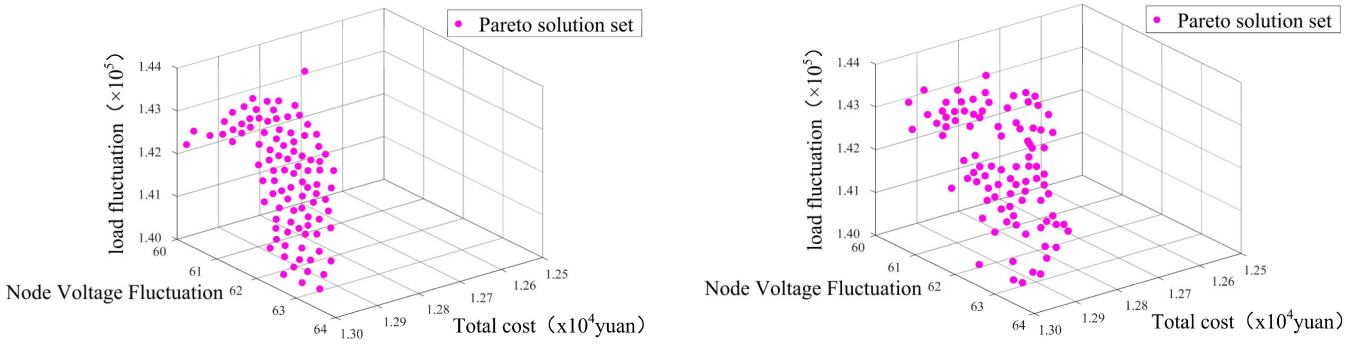

(**a**) Scenario 2 (**b**) Scenario 4

Figure 12. Pareto solution set distribution.

Through the comparison of scenes, it is obvious that the optimization results of the IMOPSO algorithm are obviously better than the MOPSO algorithm, and the search accuracy is higher. In order to compare the performance of the two algorithms, the external solution set and the spacing S are used in this paper to measure the optimization performance of the two algorithms. The S index refers to whether the particles in the Pareto solution set are evenly distributed in space. The mean variance of the particle density distance is used in this paper to characterize the uniformity and global nature of the population particles, as shown in Equation (23).

$$S = \sqrt{\frac{1}{N}\sum_{i=1}^{N}[I(x_i) - \overline{I}]^2} \tag{23}$$

where $\overline{I}$ represents the average of all particles $I(x_i)$ in the Pareto solution set.

According to the different internal environments of the two algorithms, after 20 cycles, the node voltage and load fluctuations in the optimization target are taken as the research object, as shown in Figure 13 and Table 6.

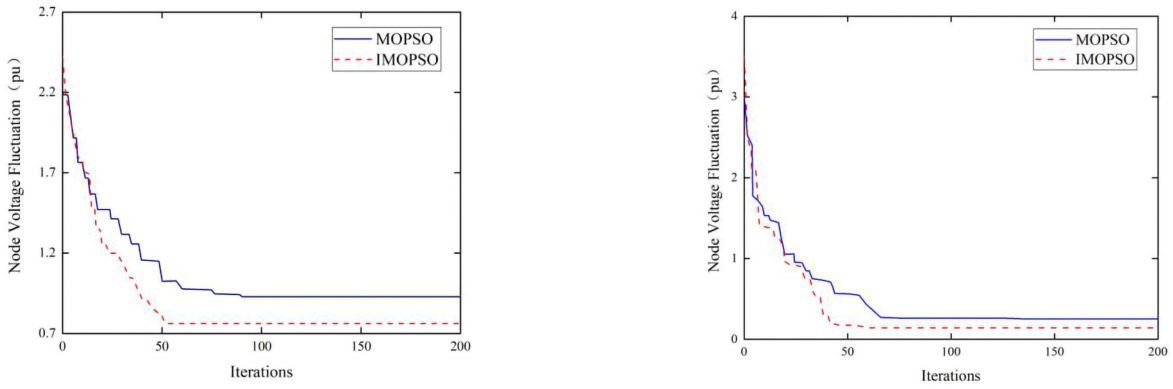

(**a**) Node Voltage Fluctuation (**b**) Load fluctuation

Figure 13. Convergence curves of external solutions for different objectives.

Table 6. Algorithm performance comparison.

Algorithm	External Solution		Distance 'S'
	Node Voltage Fluctuation	Load Fluctuation	
MOPSO	0.8869	0.2103	0.0485
IMOPSO	0.7154	0.1226	0.0317

By combining and comparing the charts, it was concluded that the IMOPSO algorithm proposed in this paper reduces the number of iterations in the node voltage fluctuation and load fluctuation, and the convergence performance is obviously better than the MOPSO algorithm. In addition, the improved algorithm and Pareto solution set update strategy make the solution set distribution more uniform and the type of solution set more diverse, and the improved MOPSO has better robustness and convergence.

5.3. Energy Storage Benefit Analysis under Different Photovoltaic Permeability

In order to verify the effectiveness of the dual-layer multi-objective optimal configuration model of the energy storage system proposed in this paper in the high-light volt permeability distribution network, the upper limit of photovoltaic power generation permeability was set at 60%, and the verification started from 30% permeability. Using the optimal configuration strategy of the BESS, the curve as shown in Figure 14 was obtained.

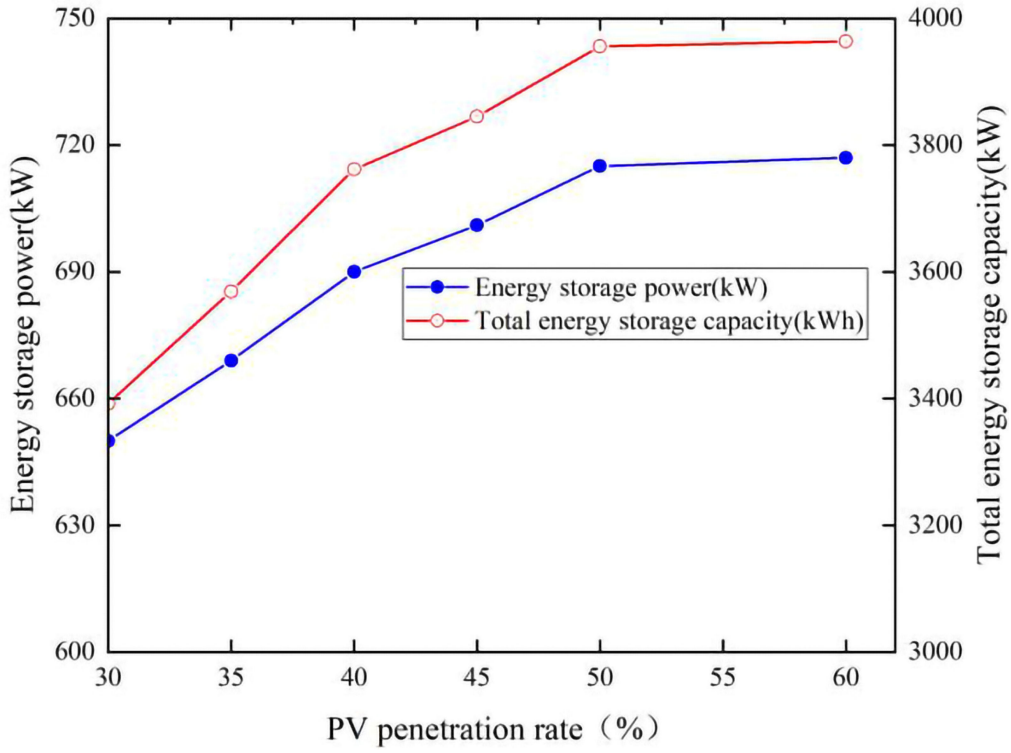

Figure 14. Changes in energy storage capacity and power under different photovoltaic penetration rates.

When the photovoltaic permeability increases from 30% to 60%, the capacity and power of the energy storage system have an obvious rising trend. When the photovoltaic permeability reaches 50%, the growth slows down and tends to remain unchanged. In other words, it is of little significance to increase the capacity of the energy storage system when the permeability reaches a certain level.

Figure 15 below shows the variation trend of energy storage investment and the total cost of distribution network operation under different photovoltaic permeability. It can be clearly seen that the total cost of the system decreases first and then increases when the photovoltaic permeability increases, and the total cost is the minimum when the permeability is 45%. As the cost of photovoltaic power generation decreases with the continuous increase of the permeability but is limited by the load level, the cost of the energy storage system increases with the increase of the capacity. The interaction between the two makes the total cost of the system decrease to the minimum when the photovoltaic permeability is 45%. When the permeability increases again, the system's total cost will keep rising, and the system operation economy will be seriously affected.

Based on the discussion of the above two legends, it is found that the total capacity of the BESS should be controlled in the optimal range according to the actual situation, and the photovoltaic permeability should also be controlled at a certain value so as to ensure the system operation economy while ensuring the safe and stable operation of the system. In order to improve the overall economy of the system, this paper selected 45% photovoltaic permeability to verify and analyze the two-layer programming model of the energy storage system proposed in this paper.

As shown in Figure 16 below, after optimizing the configuration of the energy storage system with 45% photovoltaic permeability, the load curve of the distribution network presents an obvious smoothing trend, and the peak–valley difference decreases. The sufficiency proves that the two-layer optimal configuration model of energy storage can still effectively improve the off-peak load, reduce the peak load of the distribution network,

and increase the scheduling flexibility of the distribution network under the condition of high photovoltaic permeability.

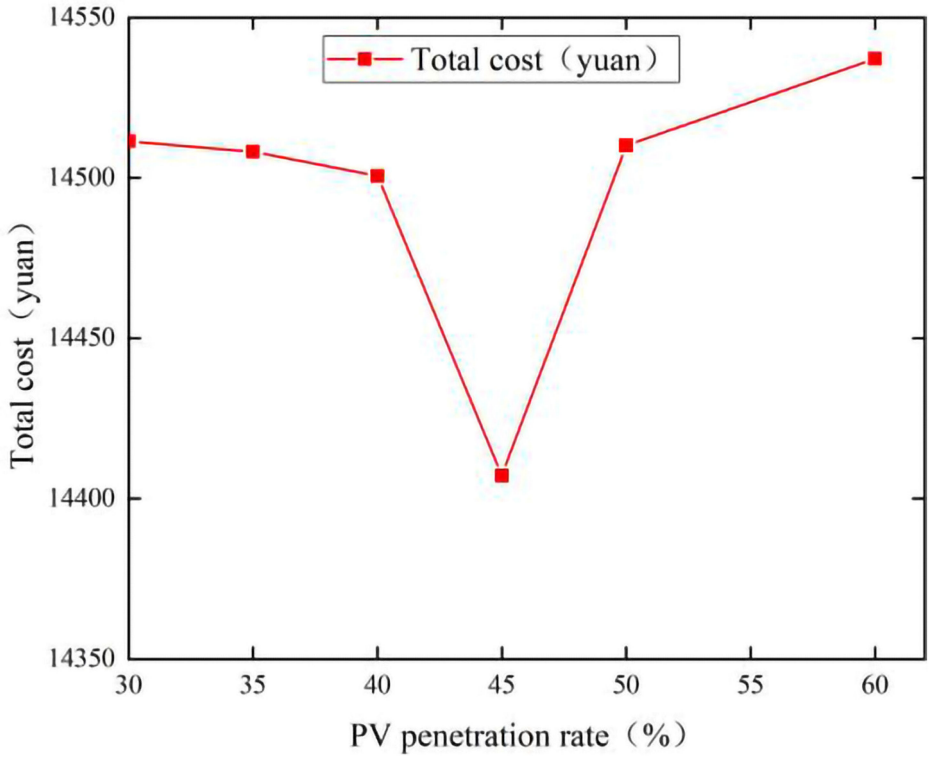

Figure 15. Total cost curve under different PV penetration rates.

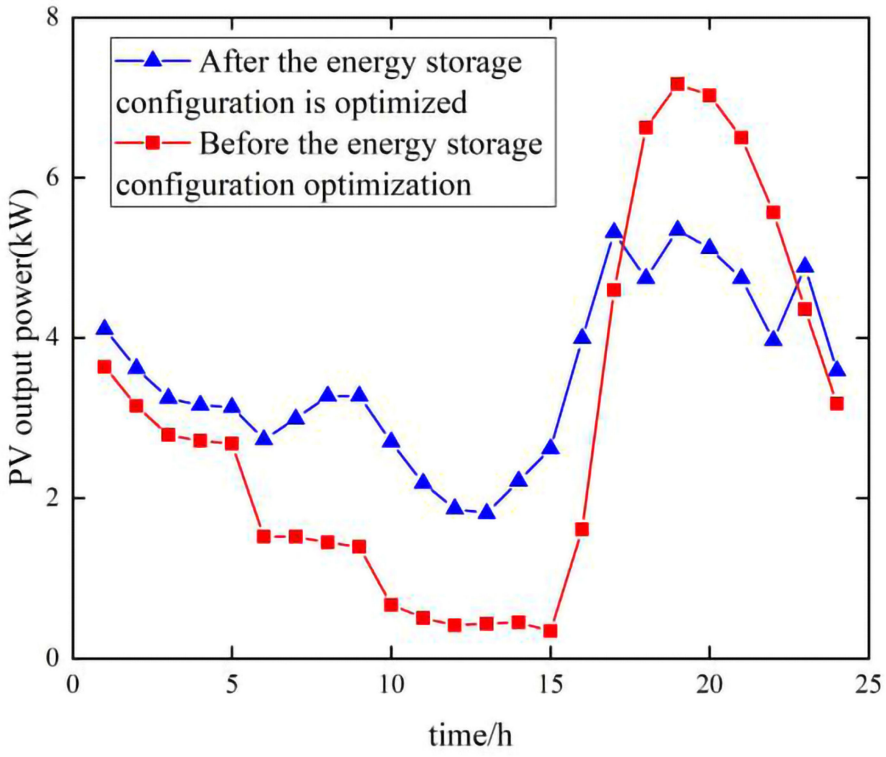

Figure 16. Distribution network load curve before and after energy storage configuration optimization under 45% photovoltaic penetration rate.

6. Conclusions

In order to ensure the power quality and scheduling flexibility of the photovoltaic distribution network with increasing permeability, this paper proposes a joint optimization operation mode of optical storage. Firstly, the PV output model was analyzed, and the scenario planning method was applied. The K-means clustering algorithm was used to divide the output scenarios, and the typical output scenarios were selected for analysis. A BESS two-layer decision model was established, and the improved IMOPSO algorithm was used to solve the two-layer model. The IEEE-33 node example was adopted, and the simulation verification was carried out based on the current feed-in price, selected energy storage parameters, and other parameters. The simulation analysis results are as follows:

① Access to energy storage can effectively smooth the load fluctuation and voltage fluctuation of system nodes in a photovoltaic distribution network. In a distribution network with high-light volt permeability, energy storage can effectively improve the off-peak load of the distribution network and reduce the peak load, thus increasing the scheduling flexibility of the distribution network.

② The bi-level programming model proposed in this paper has a good optimization ability for the rational allocation of energy storage.

③ The improved IMOPSO in this paper has good convergence performance and robustness and has good applicability in application optimization

④ When the optimal energy storage capacity under different photovoltaic permeability is configured, the total cost of the system is optimal when the photovoltaic permeability is 45%, and when the permeability increases again, the total cost of the system will keep rising and seriously affect the operation economy of the system. The analysis of this paper provides a theoretical basis for the optimal configuration of the energy storage system and an important reference for the safe, stable, and economic operation of a high permeability photovoltaic distribution network.

7. Future Work

In this paper, only batteries are considered in the selection of batteries in the energy storage system. However, with a wider application of energy storage, a single energy storage system may not be able to meet the actual demand in the future. In subsequent research, we will combine other types of energy storage for optimization analysis of hybrid energy storage.

At the same time, because of the variety of renewable energy, more and more distributed power is connected to the distribution network. This paper only analyzes access to photovoltaic power generation. In a follow-up study, we will conduct a further study on scenarios with access to various energy sources.

In addition to the voltage fluctuation and load fluctuation considered in this paper, the power system with energy storage access has more indicators to measure security. In a follow-up study, we will also analyze the improvement and influence of energy storage access on various indicators.

Author Contributions: Conceptualization, J.Z. and L.Z.; methodology, S.Z.; software, S.Z. and L.Z.; validation, J.Z., S.Z. and L.Z.; formal analysis, J.Y.; investigation, L.L.; resources, J.Y.; data curation, J.Y.; writing—original draft preparation, L.Z.; writing—review and editing, J.Z.; visualization, L.L.; supervision, J.Y. All authors have read and agreed to the published version of the manuscript.

Funding: This work is supported in part by the National Key Research and Development Program Project (Grant number: 2019YFE0104800), Natural Science Foundation of Henan Province (Grant number: 202300410271) and the Key Project of Science and Technology in Colleges and Universities of Henan Province (Grant number: 162102110130).

Data Availability Statement: The original contributions presented in the study are included in the article; further inquiries can be directed to the corresponding author.

Conflicts of Interest: The authors declare no conflict of interest.

References

1. Yao, M.; Cai, X. An Overview of the Photovoltaic Industry Status and Perspective in China. *IEEE Access* **2019**, *7*, 181051–181060. [CrossRef]
2. Jothibasu, S.; Dubey, A.; Santoso, S. Two-Stage Distribution Circuit Design Framework for High Levels of Photovoltaic Generation. *IEEE Trans. Power Syst.* **2019**, *34*, 5217–5226. [CrossRef]
3. Pan, W.; Mao, M.; Zhou, Y.; Quan, X.; Li, Y. The impact of extreme weather condition on the voltage regulation in distribution systems with high penetration of roof-top photovoltaic. *Energy Rep.* **2021**, *7*, 320–331. [CrossRef]
4. Chidurala, A.; Saha, T.K.; Mithulananthan, N. Harmonic impact of high penetration photovoltaic system on unbalanced distribution networks—Learning from an urban photovoltaic network. *IET Renew. Power Gener.* **2016**, *10*, 485–494. [CrossRef]
5. Karimi, M.; Mokhlis, H.; Naidu, K.; Uddin, S.; Bakar, A. Photovoltaic penetration issues and impacts in distribution network – A review. *Renew. Sustain. Energy Rev.* **2016**, *53*, 594–605. [CrossRef]
6. Gandhi, O.; Rodríguez-Gallegos, C.D.; Zhang, W.; Reindl, T.; Srinivasan, D. Levelised cost of PV integration for distribution networks. *Renew. Sustain. Energy Rev.* **2022**, *169*, 112922. [CrossRef]
7. Dhivya, S.K.; Anurag, S.; Dipti, S.; Reindl, T. Stability implications of bulk power networks with large scale PVs. *Energy* **2019**, *187*, 115927.
8. Maharjan, S.; Dhivya, S.K.; Khambadkone, A.M. Enhancing the voltage stability of distribution network during PV ramping conditions with variable speed drive loads. *Appl. Energy* **2020**, *264*, 114733. [CrossRef]
9. Garmabdari, R.; Moghimi, M.; Yang, F.; Lu, J. Multi-objective energy storage capacity optimisation considering Microgrid generation uncertainties. *Int. J. Electr. Power Energy Syst.* **2020**, *199*, 105908. [CrossRef]
10. Kamaruzzaman, Z.A.; Mohamed, A. Dynamic voltage stability of a distribution system with high penetration of grid-connected photovoltaic type solar generators. *J. Electr. Syst.* **2016**, *12*, 239–248.
11. Xu, Z.; Yuan, B.; Liu, J.; Zheng, K.; Xu, S. Energy storage configuration for smoothing the output volatility of PV power generation. *IOP Conf. Ser. Earth Environ. Sci.* **2019**, *295*, 052045. [CrossRef]
12. Rana, M.M.; Uddin, M.; Sarkar, M.R.; Shafiullah, G.M.; Huadong, M.; Atef, M. A review on hybrid photovoltaic—Battery energy storage system: Current status, challenges, and future directions. *J. Energy Storage* **2022**, *51*, 104597. [CrossRef]
13. Haytham, M.A.A.; Ahmed, S.A.A.; Mohamed, H.A.; Salama, M.M.A. Mitigating voltage-sag and voltage-deviation problems in distribution networks using battery energy storage systems. *Electr. Power Syst. Res.* **2020**, *184*, 106294.
14. Amini, M.; Khorsandi, A.; Vahidi, B.; Hosseinian, S.H.; Malakmahmoudi, A. Optimal sizing of battery energy storage in a microgrid considering capacity degradation and replacement year. *Electr. Power Syst. Res.* **2021**, *195*, 107170. [CrossRef]
15. Hossain, S.J.; Biswas, B.D.; Bhattarai, R.; Ahmed, M.; Abdelrazek, S.; Kamalasadan, S. Operational Value Based Energy Storage Management for Photo-Voltaic(PV) Integrated Active Power DistributionSystems. *IEEE Trans. Ind. Appl.* **2019**, *99*, 5320–5330. [CrossRef]
16. Koohi-Fayegh, S.; Rosen, M.A. A review of energy storage types, applications and recent developments. *J. Energy Storage* **2020**, *2*, 101047. [CrossRef]
17. Chang, L.; Zhuo, J.; Zhao, D.; Li, S.; Chen, J.; Wang, J.; Yao, Q. A review on Flexible and safe operation of renewable energy microgrid using energy storage system. *Proc. CSEE* **2020**, *1*, 1–18+369.
18. Rajamand, S.; Miadreza, S.-K.; Catalão, J.P.S. Energy storage systems implementation and photovoltaic output prediction for cost minimization of a Microgrid. *Electr. Power Syst. Res.* **2022**, *202*, 107596. [CrossRef]
19. Rahman, S.; Saha, S.; Haque, M.E.; Islam, S.N.; Arif, M.T.; Mosadeghy, M.; Oo, A.M.T. A framework to assess voltage stability of power grids with high penetration of solar PV systems. *Int. J. Electr. Power Energy Syst.* **2022**, *139*, 107815. [CrossRef]
20. Zhao, L.; Zhang, T.; Peng, X.; Zhang, X. A novel long-term power forecasting based smart grid hybrid energy storage system optimal sizing method considering uncertainties. *Inf. Sci.* **2022**, *610*, 326–344. [CrossRef]
21. Liang, J.; Lan, F.; Li, J. A grid scenario evaluation method for energy storage capacity demand of photovoltaic-based distribution network. *Autom. Electr. Power Syst.* **2018**, *42*, 40–47+85.
22. Shoaib, B.; Muhammad, A.; Muqeet Hafiz, A.; Muhammad, S.; Harun, J.; Monia, H.; Sattar, M.A.; Habib, H. Optimal Scheduling of Demand Side Load Management of Smart Grid Considering Energy Efficiency. *Front. Energy Res.* **2022**, *10*, 861571.
23. Waseem, M.; Lin, Z.; Liu, S.; Sajjad, I.A.; Aziz, T. Optimal GWCSO-based home appliances scheduling for demand response considering end-users comfort. *Electr. Power Syst. Res.* **2020**, *187*, 106477. [CrossRef]
24. Rezaeimozafar, M.; Eskandari, M.; Hadi Amini, M.; Moradi, M.H.; Siano, P. A Bi-Layer Multi-Objective Techno-Economical Optimization Model for Optimal Integration of Distributed Energy Resources into Smart/Micro Grids. *Energies* **2020**, *13*, 1706. [CrossRef]
25. Waseem, M.; Lin, Z.; Liu, S.; Zhang, Z.; Aziz, T.; Khan, D. Fuzzy compromised solution-based novel home appliances scheduling and demand response with optimal dispatch of distributed energy resources. *Appl. Energy* **2021**, *290*, 116761. [CrossRef]
26. Li, D.; Cai, W. Optimal configuration of photovoltaic energy storage capacity for large power users. *Energy Rep.* **2021**, *7* (Suppl. S7), 468–478. [CrossRef]
27. Yang, P.; Nehorai, A. Joint Optimization of Hybrid Energy Storage and Generation Capacity with Renewable Energy. *IEEE Trans. Smart Grid* **2014**, *5*, 1566–1574. [CrossRef]
28. Wu, J.; Wen, C.; Li, S.; Shi, Q. Capacity optimization allocation of photovoltaic energy storage system based on TOU. *Adv. Technol. Electr. Eng. Energy* **2018**, *37*, 23–30.

29. Lima, D.A.; Feijão, V.R. Stochastic approach for economic viability of photovoltaic systems with battery storage for big electricity consumers in the regulated marketin Brazil. *Electr. Power Syst. Res.* **2022**, *205*, 107744. [CrossRef]
30. Guo, Y.; Xiang, Y. Cost–benefit analysis of photovoltaic-storage investment in integrated energy systems. *Energy Rep.* **2022**, *8* (Suppl. S5), 66–71. [CrossRef]
31. Lu, S.; Wang, X.; Wu, J. Location and Size Planning of Distributed Photovoltaic Generation in Distribution network System Based on K-means Clustering Analysis. *IOP Conf. Ser. Earth Environ. Sci.* **2018**, *108*, 052022. [CrossRef]
32. Home-Ortiz, J.M.; Pourakbari-Kasmaei, M.; Lehtonen, M.; Sanches Mantovani, J.R. Optimal location-allocation of storage devices and renewable-based DG in distribution systems. *Electr. Power Syst. Res.* **2019**, *172*, 11–21. [CrossRef]
33. Wang, W.; Dou, F.; Yu, X.; Liu, G. Scenario analysis of wind power output based on improved k-means algorithm. *IOP Conf. Ser. Earth Environ. Sci.* **2021**, *675*, 012092. [CrossRef]
34. Liang, G.; Sun, B.; Zeng, Y.; Ge, L.; Li, Y.; Wang, Y. An Optimal Allocation Method of Distributed PV and Energy Storage Considering Moderate Curtailment Measure. *Energies* **2022**, *15*, 7690. [CrossRef]
35. Feng, J.; Zhou, H. Bi-Level Optimal Capacity Planning of Load-Side Electric Energy Storage Using an Emission-Considered Carbon Incentive Mechanism. *Energies* **2022**, *15*, 4592. [CrossRef]
36. Feng, H.; Ma, W.; Yin, C.; Cao, D. Trajectory control of electro-hydraulic position servo system using improved PSO-PID controller. *Autom. Constr.* **2021**, *127*, 103722. [CrossRef]
37. Wang, G.; Wan, Z.; Wang, X. Review of two (double) level planning. *Adv. Math.* **2007**, *5*, 513–529.
38. Gong, Z. Study on Two-Stage Optimal Scheduling Strategy and Time-of-Use Price Optimization of Optical Storage System. Master's Thesis, Hefei University of Technology, Hefei, China, 2021.